


Johns-Rahnejat, P.M., Dolatabadi, N. and Rahnejat, H., "Contact mechanics of highly loaded counterformal finite line contacts: Semi-infinite and layered elastic solids", Proc. Lubrication, Maintenance and Tribotechnology (LUBMAT 2023), 17-19th July 2023, Preston, UK, 10 pp.

Contact Mechanics of Highly Loaded Counterformal Finite Line Contacts: Semi-Infinite and Layered Elastic Solids

P.M. Johns-Rahnejat¹ , N. Dolatabadi^{2*}  and H. Rahnejat^{1,2} 

¹School of Engineering, University of Central Lancashire, Preston, UK

²Wolfson School of Mechanical, Electrical and Manufacturing Engineering, Loughborough University, Loughborough, UK

*Corresponding Author: N.Dolatabadi@lboro.ac.uk

Keywords: Tribo-technology, Contact mechanics, Modelling, Machine element operation

Abstract

Increasingly, machines operate under harsh contact conditions with high normal contact loads and tangential traction. This leads to increased wear and contact fatigue. Sub-surface stresses are responsible for premature contact fatigue failure of rolling element bearings, meshing gear teeth and cam-follower pairs. Consequently, surface protection measures, including hard wear-resistant coatings, have become commonplace. The choice of protective layers, method of fabrication, geometry and contact conformity affect fatigue performance. Traditionally, the prediction of contact integrity has been made using classical Hertzian contact mechanics. However, the theory is only applicable when the contact of a solid pair may be considered as an ellipsoidal indenter penetrating a semi-infinite elastic half-space, which is not the case for thin coatings.

The paper provides comprehensive generic contact mechanics analysis with induced sub-surface stresses in concentrated counterformal contacts for both semi-infinite and layered bonded elastic solids at high loads.

Introduction

Rolling element bearings are used in many applications. They are usually subjected to high, variable and often impulsive loads, for example in the meshing gear pairs of automotive transmissions or differentials [1, 2] or in wind turbines which are subjected to external variable wind and gust loading [3]. Variations in the applied and impulsive loads and in some cases misalignment of bearing elements can cause excessive contact stresses that often result in the fatigue of surfaces and failure of bearings [4, 5]. Bearing surfaces subjected to fatigue spalling and pitting lead to structural impairment issues and poor system reliability and operational performance. With ever increasing harsh operational conditions, such as in wind turbines' transmissions, there are high incidences of bearing failure [4,6]. These require costly repair and result in inordinate system downtimes. Detailed contact mechanics, particularly the evaluation of induced sub-surface stresses, is therefore essential in design evaluation and prediction of system performance [7-10]. These stresses are affected by contact conformity [11, 12] as well as by surface materials. Thin elastic hard wear-resistant coatings, for example, should be treated as bonded layered solids [12-15]. Hence, accurate predictions of contact stresses and failure require the development and

use of appropriate predictive methodologies. This paper presents detailed contact mechanics for the case of finite line contacts, and sub-surface stress evaluation for both semi-infinite elastic solids and thin bonded layers.

Contact Mechanics of Semi-infinite Finite Line Contacts

The contact of a rolling element bearing-to-raceway is considered by Hertzian contact mechanics to be a rigid roller with a reduced radius, R , indenting a semi-infinite elastic half-space with an equivalent reduced elastic modulus, E^* (see figure 1):

$$\frac{1}{R} = \frac{1}{R_1} + \frac{1}{R_2} \quad (1)$$

and:

$$\frac{1}{E^*} = \frac{1-\nu_1^2}{E_1} + \frac{1-\nu_2^2}{E_2} \quad (2)$$

The roller imprints a long, narrow rectangular strip (footprint) into the semi-infinite elastic half-space. This contact configuration is termed an elastic line contact with a half-width of a_0 :

$$a_0 = \left\{ \frac{2}{\pi E^*} \frac{WD}{L} \right\}^{1/2} \quad (3)$$

The lateral cross-sectional pressure profile is assumed to be elliptical, with a uniform longitudinal pressure distribution (figure 1). The central pressure is:

$$p_0 = \frac{2W}{\pi a_0 L} \quad (4)$$

The parabolic approximation of the cross-sectional elliptical pressure profile is:

$$p(x, y) = p_0 \left\{ 1 - \left(\frac{x}{a_0} \right)^2 \right\}^{1/2} \quad (5)$$

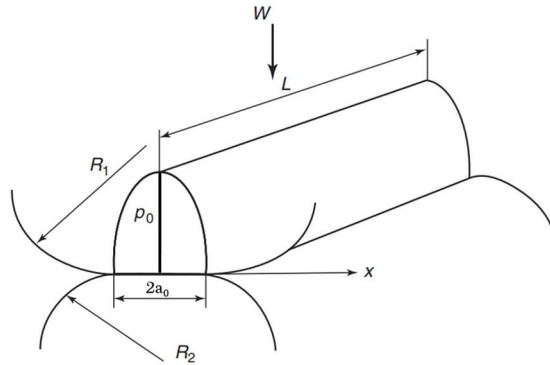


Figure 1: Idealised elastic line contact of cylindrical solids of revolution

The deflection anywhere within the thin contact footprint can be obtained as:

$$\delta(x, y) = \frac{1}{\pi E^*} \int_{-a_0}^{a_0} \int_{-\frac{L}{2}}^{\frac{L}{2}} \frac{p(x_1, y_1)}{\{(x-x_1)^2 + (y-y_1)^2\}^{1/2}} dx_1 dy_1 \quad (6)$$

where: $E^* = \frac{E}{1-\nu^2}$ for contacting surfaces of the same material (plane strain effective modulus).

The central contact deflection becomes [16]:

$$\delta_0(0,0) = \frac{a_0 p_0}{\pi E^*} \left\{ \ln \frac{2L}{a_0} + \frac{1}{2} \right\} \quad (7)$$

Therefore, the footprint of an elastic line contact is fully described by the classical Hertzian contact theory [17]. However, the infinite elastic line contact is idealised. In practice, a rigid roller indents an elastic half-space with a dog-bone (dumbbell) shaped footprint, the contact extremities spreading out due to the sharp-end stress discontinuity (figure 2). In this case the contact configuration is termed finite line contact, and a numerical approach is required to obtain the pressure distribution. A number of numerical solutions have been reported, including the initial solutions for the case of elastostatic contact of cylindrical roller bearings under assumed dry contact condition [18--20]. There have also been various solutions of elastohydrodynamic lubricated finite line contacts under aligned, misaligned, isothermal or thermal conditions in steady state or transient motions [21-29].

For finite line contact, a numerical solution is required. In this case the contact footprint is sub-divided into a number of overlapping rectangular elements as shown in figure 2. The local pressure distribution is assumed to be parabolic in the lateral direction and described by isosceles triangles in the longitudinal direction (figure 3). This approach takes into account parabolic approximation of the Hertzian elliptical pressure profile in the transverse direction. The deflection at any point (x, y) within a computational element is obtained as:

$$\delta(x, y) = \frac{p_m(1-\nu^2)}{\pi E} \int_{-a_1}^{a_1} \int_{-c}^c \frac{\left(1 - \frac{|y_1|}{c}\right) \left\{1 - \left(\frac{x_1}{a_1}\right)^2\right\}^{1/2}}{\{(x-x_1)^2 + (y-y_1)^2\}^{1/2}} dx_1 dy_1 \quad (8)$$

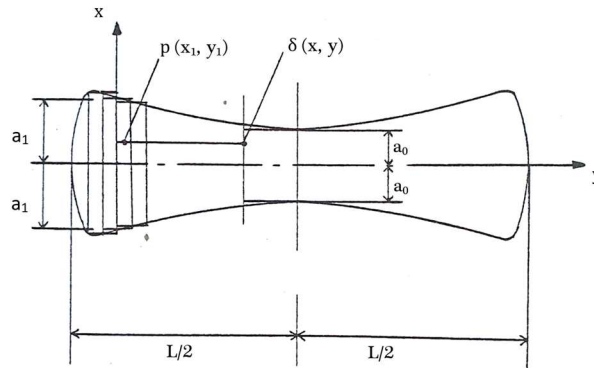


Figure 2: Dog-bone shaped footprint of finite line contact with elemental discretisation

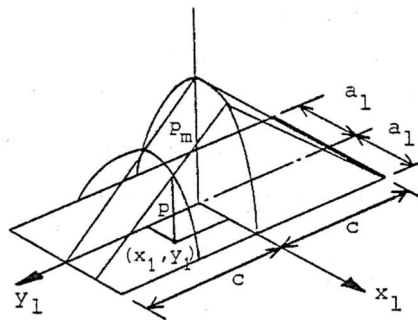


Figure 3: Computational element

The following relations are used to non-dimensionalise equation (8):

$$x = a\bar{x}, x_1 = a_1\bar{x}_1, y = c\bar{y}, y_1 = c\bar{y}_1 \text{ and } \delta = a_1\bar{\delta} \quad (9)$$

Thus:

$$\bar{\delta}(\bar{x}, \bar{y}) = p_m \frac{(1-\vartheta^2)}{\pi E} I \int_0^1 (1 - \bar{x}^2)^{1/2} d\bar{x} \quad (10)$$

where I is the integration term in the non-dimensional form of equation (8) with respect to \bar{y}_1 , yielding [18]:

$$I = \int_{-1}^1 \frac{1-|\bar{y}_1|}{\{(\bar{a}\bar{x}-\bar{a}_1\bar{x}_1)^2+(\bar{y}-\bar{y}_1)^2\}^{1/2}} d\bar{y}_1 \quad (11)$$

where: $\bar{a} = \frac{a}{c}$ and: $\bar{a}_1 = \frac{a_1}{c}$

This yields the boundary integral equation:

$$I = (\bar{y} - 1) \ln \left\{ \frac{\bar{y}-1+[(\bar{a}\bar{x}-\bar{a}_1\bar{x}_1)^2+(\bar{y}-1)^2]^{1/2}}{\bar{y}+[(\bar{a}\bar{x}-\bar{a}_1\bar{x}_1)^2+\bar{y}^2]^{1/2}} \right\} - [(\bar{a}\bar{x} - \bar{a}_1\bar{x}_1)^2 + (\bar{y} - 1)^2]^{1/2} + [(\bar{a}\bar{x} - \bar{a}_1\bar{x}_1)^2 \bar{y}^2]^{1/2} \quad (12)$$

The function in the boundary integral equation (12) is not symmetric about all the four quadrants of the computational element in figure 3. Therefore, to find the total deflection at the centre of each computational element, it is necessary to combine the contributions due to all four elemental quadrants in figure 3 as:

$$d_i(\bar{x}, \bar{y}) = \frac{a_1 p_m (1-\vartheta^2)}{\pi E} \int_0^1 (1 - \bar{x}_1^2)^{1/2} I d\bar{x}_1 \quad (13)$$

The total deflection at the centre of any rectangular computational element, j , becomes:

$$\delta_j = \sum_{k=1}^4 d_{jk} \quad (14)$$

where j is any element within a total of n overlapping rectangular elements used to discretise the contact footprint and $k = 1 \rightarrow 4$ are the quadrants in each rectangular computational element.

Using equations (13) and (14) and multiplying both sides by the term $\frac{\pi E}{a_0 p_0 (1-\vartheta^2)}$, the following relationship is obtained for the j th nodal point:

$$\frac{\pi E \delta_j}{a_0 p_0 (1-\vartheta^2)} = \sum_{i=1}^n \frac{a_i p_{mi}}{a_0 p_0} I_{ij} \quad (15)$$

where $i = 1 \rightarrow n$, and I_{ij} is obtained from equation (12).

In dimensionless form:

$$\bar{\delta}_j = \sum_{i=1}^n \bar{a}_i \bar{p}_{mi} I_{ij} \quad (16)$$

Hence, to evaluate the unknown pressure distribution:

$$[\bar{p}_{mi}] = [\bar{a}_i I_{ij}]^{-1} [\bar{\delta}_j] \quad (17)$$

The Case of Bonded Elastic Layered Solids

Increasingly, contacting surfaces are coated for a variety of reasons. Coatings include the use of thin hard wear-resistant coatings such as diamond like carbon (DLC), Alumina, Silicon Nitride, Bismuth or Indium. The contact mechanics deviate from that described above, and semi-infinite assumption cannot be upheld.

For the case of hard layered bonded elastic solids, Johnson [12] states that for the bonded layer thickness $b \ll a$ (half-width of contact footprint), plane sections remain plane, and:

$$\varepsilon_x = \frac{1-\vartheta_l^2}{E_l} \left\{ \sigma_x + \frac{\vartheta}{1-\vartheta} p(x) \right\} = 0 \quad (18)$$

$$\varepsilon_z = \frac{1-\vartheta_l^2}{E_l} \left\{ -p(x) - \frac{\vartheta}{1-\vartheta} \sigma_x \right\} \quad (19)$$

Eliminating σ_x and replacing ε_z from:

$$\varepsilon_z = -\frac{1}{b} \left(\delta - \frac{x^2}{2R} \right) \quad (20)$$

yields:

$$p(x) = \frac{1-\vartheta_l}{1-2\vartheta_l} \frac{E_l}{1+\vartheta_l} \frac{a^2}{2Rb} \left(1 - \frac{x^2}{a^2} \right) \quad (21)$$

where:

$$a = \left\{ \frac{3}{2} \frac{RbW}{L} \frac{1-2\vartheta_l}{1-\vartheta_l} \frac{1+\vartheta_l}{E_l} \right\}^{1/4} \quad (22)$$

The above relations hold true for compressible layers: $\vartheta < 0.5$, which account for most coatings. However, for incompressible layers, equation (21) returns a value of infinity, which is clearly erroneous. Johnson [12] provides expressions for incompressible layers in line contact, whilst the same for circular point contacts is provided in [15, 30].

Method of Solution

For any rigid cylinder indenting an elastic plane, a trial load is initially used to evaluate the contact conditions, a_0 and p_0 . Then, an initial estimate of central contact deflection is made for either case of semi-infinite or bonded layered elastic solid. An initial rectangular contact footprint as in idealised line contact is assumed. Any misaligned contact condition can also be taken into account, though is not considered in the current study. All negative deflections are discarded as the method is only applicable to compressive conditions. Subsequently, the influence matrix $[\bar{a}_l I_{ij}]$ is evaluated and the pressure distribution $[\bar{p}_{mi}]$ obtained. The following convergence criterion should be met:

$$|p^{new} - p^{old}| \leq \varepsilon_p \quad (23)$$

If the criterion is not satisfied, then the procedure is repeated as shown in the flowchart of figure 4.

To obtain the final solution, the equilibrium condition must be satisfied. This means that contact reaction (integrated pressure distribution) should equate to the applied contact load W within a specified error tolerance:

$$\iint p dx dy - W \leq \varepsilon_w \quad (24)$$

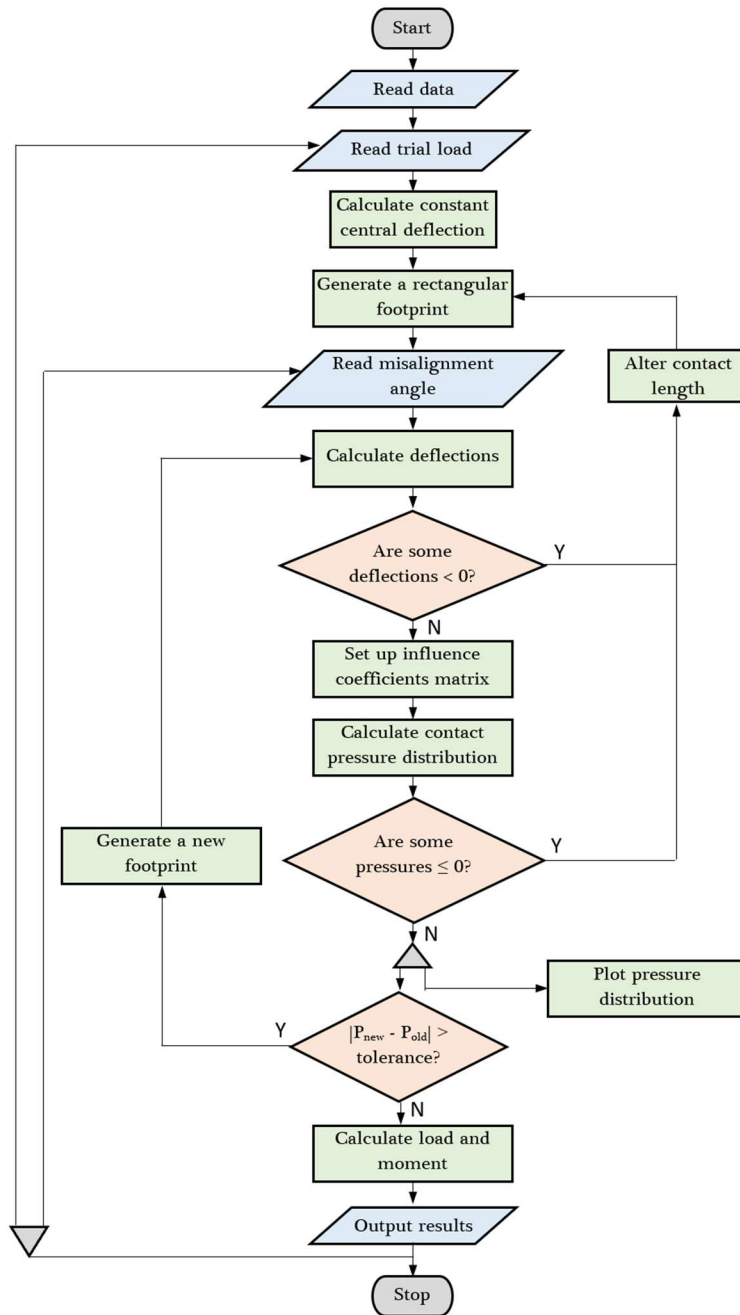


Figure 4: Computational flowchart

Determination of sub-surface stress field

Having obtained the pressure distribution, the induced sub-surface stresses which can be responsible for inelastic deformation of the contacting surfaces can be calculated. Fatigue spalling/pitting can occur when the stresses reach their elastic limit and coincide with sub-surface material flaws such as voids or inclusions. For ductile materials, the determining sub-surface stresses are the orthogonal reversing shear stresses, subjecting the material layers to repetitive cycles of compression/tension [11, 31, 32]:

$$\tau_{zx} = -\frac{2}{\pi} \bar{z}^2 p_m \int_{-1}^1 (\bar{x} - \bar{x}_1)(1 - \bar{x}^2) \{(\bar{x} - \bar{x}_1)^2 + \bar{z}^2\}^{-2} d\bar{x}_1 \quad (25)$$

where, $\bar{z} = \frac{z}{a}$ (into the depth of the contacting solid) and τ_{zx} is the sub-surface reversing orthogonal shear stress distribution in each cross section along the width of the contact, x .

Results and Discussion

Figure 5 shows a typical axial pressure profile for a straight-edged (unprofiled) roller ($R = 0.0127\text{ m}$, $L = 0.0127\text{ m}$) indenting a semi-infinite elastic half-space subjected to a contact load of 3683.6 N, based on a total bearing reaction $F \approx 10.8\text{ KN}$, obtained using [20, 33] where $N=12$:

$$W = \frac{4.08 F}{N} \quad (26)$$

This expression is for the bottom roller (the highest loaded roller) with zero clearance in a horizontal shaft and bearing system. The other rollers experience lower contact forces at any instant of time. With zero clearance, the top roller is often completely unloaded.

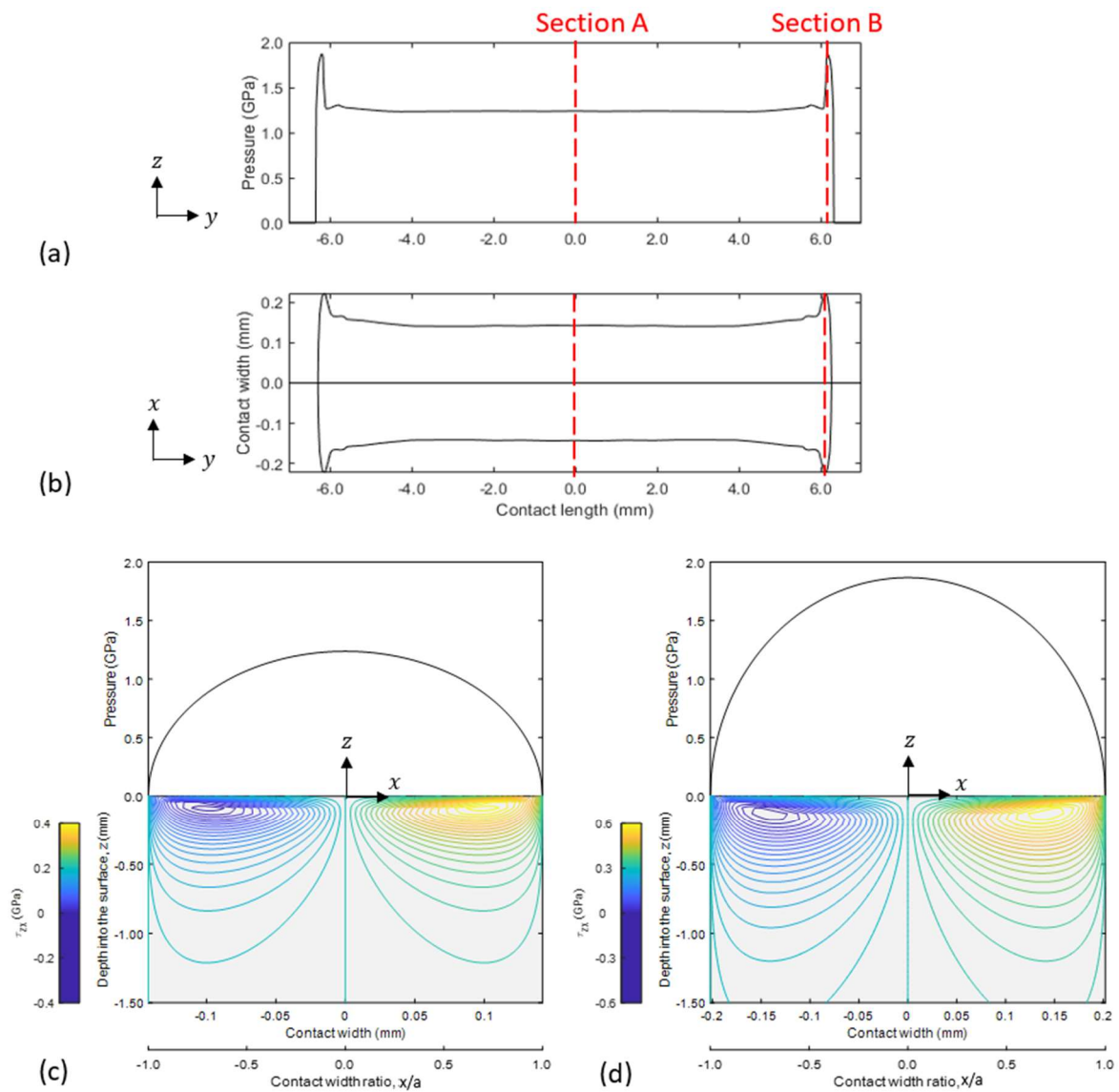


Figure 5: Contact mechanics prediction of finite line contact geometry

The footprint for a finite line contact is a dumbbell or dog-bone shape with end-extremities spreading out due to an abrupt change of profile (figure 5(b)). The lateral pressure profile

for the roller is elliptical at all cross-sections (profiles at sections A and B are shown in figures 5(c) and 5(d) respectively).

Figures 5(c) and 5(d) also show predicted sub-surface shear stresses which are often responsible for inelastic deformation. Note: $\tau_{zx} = 0$ along the footprint longitudinal axis.

Owing to the progressively harsh operating conditions, bearings are often coated with protective hard layers. Data regarding some of these hard coatings are listed in table 1. Cobalt-chromium bearing steel is included in the table as it is the usual substrate material. All coatings have a similar modulus of elasticity to the bearing steel, but they are much harder. Due to this and their thinness, the contact footprint is much narrower (in the lateral x -direction) when the bearing is subjected to the same contact load, and correspondingly much higher pressures are generated. This is shown in Figure 6 for the same roller dimensions and contact load as that in figure 5.

The results in figure 6 demonstrate that whilst the semi-infinite elastic assumption (Neo-Hertzian analysis) is appropriate for the steel roller, it clearly leads to serious erroneous predictions for thin coatings (large differences in pressures between semi-infinite and layered bonded solid analysis).

Table 1: Mechanical properties of solid half space and layered solids

Material	Modulus of Elasticity, E (GPa)	Poisson's ratio	Layer thickness, b (μm)
Steel	206	0.30	--
Si ₃ N ₄	250	0.20	6
Al ₂ O ₃	300	0.21	3
DLC	220	0.21	2

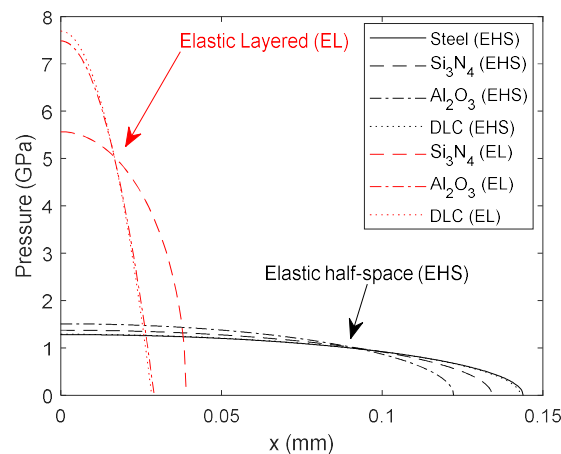


Figure 6: Comparison of generated pressure distribution for semi-infinite and layered bonded solid (coated) surfaces (half symmetric lateral pressure profiles at the contact centre are shown)

For example, in the case of alumina and DLC coated rollers, the generated pressures are almost five times higher than when the coatings are considered to be semi-infinite elastic half-spaces. Correspondingly, the contact semi-half-width is nearly a quarter of that for a semi-infinite assumption. This means that contact footprint is reduced with hard coatings, whilst the generated pressures significantly increase (the area under the distributions remain the same, representing the applied contact load).

Failure of hard coatings are often through fracture when maximum shear stress exceeds the condition prescribed by the Tresca criterion:

$$\tau_{max} = 0.3p_0 \geq \frac{\sigma_Y}{2} \quad (27)$$

In particular, coatings can exfoliate from the substrate if this maximum shear stress coincides with the interfacial layer between the coating and the substrate. Although the generated pressures are quite large (p_0 values in figure 6), the Tresca criterion is not readily reached because the elastic limit, σ_Y , is high for these hard coatings, for example $\sigma_Y = 10 \text{ GPa}$ for alumina. Thus, for alumina as a layered bonded solid in figure 6: $\tau_{max} = 0.3p_0 = 2.25 \text{ GPa} < \frac{\sigma_Y}{2} \approx 5 \text{ GPa}$.

Concluding Remarks

The paper shows that it is essential to use appropriate contact mechanics analysis to accurately predict prevailing conditions for thin coated surfaces. The use of idealised infinite line contacts with semi-infinite elastic half-space analysis can lead to significant errors.

Acknowledgements

The authors wish to express their gratitude to the Science Research Council (now EPSRC) and the Ministry of Defence, Royal Aircraft Establishment (RAE) for their financial support resulting in the development of some of the methodologies used in this paper.

Nomenclature

Roman Symbols:

a_0	Semi-half-width at the centre of the contact
a_1	Semi-half-width at any contact cross-section
b	Layer thickness
c	Half-width of rectangular computational element
D	Roller diameter
E	Effective Young's modulus of elasticity
E_1, E_2	Modulus of elasticity of contacting bodies
E_l	Modulus of elasticity of the layer
E^*	Effective elastic modulus of the contact
F	Bearing reaction
L	Length roller (Contact footprint length)
N	Number of rollers in the bearing
n	Number of computational elements
p	Pressure
p_0	Central contact pressure

p_m	Maximum pressure of any computational element
R	Effective contact radius
W	Contact load
x, y	Co-ordinates of a point of deflection
x_1, y_1	Co-ordinates of a point of pressure
z	Co-ordinate into the depth of elastic solid

Greek Symbols:

δ	Deflection
δ_0	Deflection at the centre of the contact
ε_p	Limit of convergence for pressures
ε_w	Limit of convergence for elastostatic equilibrium
ϑ	Poisson's ratio
ϑ_l	Poisson's ratio for the layer
τ_{zx}	Orthogonal reversing shear stress
τ_{max}	Maximum shear stress

References

- [1] Mohammadpour, M., Johns-Rahnejat, P.M., Theodossiades, S. and Rahnejat, H., "Effect of tapered roller bearing supports on the dynamic behaviour of hypoid gear pair differentials", Proc. IMechE, Part D: J. Automobile Engineering, 2016, 230(8), pp. 1090-1104.

- [2] Sivayogan, G., Dolatabadi, N., Johns-Rahnejat, P., Rahmani, R. and Rahnejat, H., "Non-Newtonian Thermo-Elastohydrodynamics and Sub-Surface Stress Field of High-Performance Racing Spur Gears", *Lubricants*, 2022, 10(7):146.
- [3] Márquez, F.P., Tobias, A.M., Pérez, J.M. and Papaalias, M., "Condition monitoring of wind turbines: Techniques and methods", *Renewable Energy*, 2012, 46, pp. 169-178.
- [4] Greco, A., Sheng, S., Keller, J. and Erdemir, A., "Material wear and fatigue in wind turbine systems", *Wear*, 2013, 302(1-2), pp. 1583-1591.
- [5] Liu, Z. and Zhang, L., "A review of failure modes, condition monitoring and fault diagnosis methods for large-scale wind turbine bearings", *Measurement*, 2020, 149:107002.
- [6] Yucesan, Y.A. and Viana, F.A., "A physics-informed neural network for wind turbine main bearing fatigue", *Int. J. Prognostics and Health Management*, 2020, 11, pp. 1-17.
- [7] Johns-Rahnejat, P.M. and Gohar, R., "Point contact elastohydrodynamic pressure distribution and sub-surface stress field", In *Tri-annual Conf. on Multi-body Dynamics: monitoring and simulation techniques*, Bradford, UK, 1997.
- [8] Harris, T.A. and Yu, W.K., "Lundberg-Palmgren fatigue theory: considerations of failure stress and stressed volume", *J. Tribology*, 1999, 121(1), pp. 85-89.
- [9] Slack, T. and Sadeghi, F., "Explicit finite element modeling of subsurface initiated spalling in rolling contacts", *Tribology International*, 2010, 43(9), pp. 1693-1702.
- [10] Rahnejat, H., Rahmani, R., Mohammadpour, M. and Johns-Rahnejat, P.M., "Tribology of power train systems", *ASM Handbook*, 2017, 18, pp. 916-934.
- [11] Johns-Rahnejat, P.M., Dolatabadi, N. and Rahnejat, H., "Analytical elastostatic contact mechanics of highly-loaded contacts of varying conformity", *Lubricants*, 2020, 8(9):89.
- [12] Johnson, K.L., "Contact Mechanics", Cambridge University Press, Cambridge, 1985.
- [13] G.R. Naghieh, G.R., Rahnejat, H., Jin, Z.M., "Characteristics of frictionless contact of bonded elastic and viscoelastic layered solids", *Wear*, 1998, 232, pp. 243-249
- [14] K. Konvopoulos, K. and Gong, Z.Q., "Effect of surface patterning on contact deformation of elastic-plastic layered media", *J. Tribology*, 2003, 125, pp. 16-24
- [15] Teodorescu, M., Rahnejat, H., Gohar, R. and Dowson, D., "Harmonic decomposition analysis of contact mechanics of bonded layered elastic solids", *Applied Mathematical Modelling*, 2009, 33(1), pp. 467-485.
- [16] Johns, P.M., "The design of cylindrical rollers for use in shaft and bearing systems", *Diss. MSc Thesis*, Imperial College of Science and Technology, London, 1978.
- [17] Hertz, H., "The contact of elastic solids", *J. Reine Angew. Math.* 1881, 92, pp. 156-171.
- [18] Kannel, J.W., "Comparison Between Predicted and Measured Axial Pressure Distribution Between Cylinders", *J. Lubrication Tech.*, 1974, 96, pp. 508-514
- [19] Heydari, M. and Gohar, R., "The Influence of the Axial Profile on Pressure Distribution in Radially Loaded Rollers", *J. Mechanical Engineering Science*, 1979, 21(6), pp. 381-388
- [20] Johns, P.M. and Gohar, R., "Roller bearings under radial and eccentric loads. *Tribology International*", 1981, 14(3), pp. 131-136.
- [21] Mostofi, A. and Gohar, R., "Elastohydrodynamic lubrication of finite line contacts", *J. of Lubrication Tech.*, 1983, 105(4), pp. 598-604.
- [22] Park, T.J. and Kim, K.W., "Elastohydrodynamic lubrication of a finite line contact", *Wear*, 1998, 223(1-2), pp. 102-109.
- [23] Johns-Rahnejat PM, Karami G, Aini R, Rahnejat H. Fundamentals and advances in elastohydrodynamics: The role of Ramsey Gohar. *Lubricants*. 2021 Dec;9(12):120.
- [24] Kushwaha, M., Rahnejat, H. and Gohar, R., "Aligned and misaligned contacts of rollers to races in elastohydrodynamic finite line conjunctions", *Proc. IMechE, Part C: J. Mechanical Engineering Science*, 2002, 216(11), pp. 1051-1070.
- [25] Liu, X. and Yang, P., "Analysis of the thermal elastohydrodynamic lubrication of a finite line contact", *Tribology International*, 2002, 35(3), pp. 137-144.
- [26] Kushwaha, M. and Rahnejat, H., "Transient concentrated finite line roller-to-race contact under combined entraining, tilting and squeeze film motions", *J. Physics, D: Applied Physics*, 2004, 37(14):2018.
- [27] Rahnejat, H., Johns-Rahnejat, P.M., Teodorescu, M., Votsios, V. and Kushwaha, M., "A review of some tribodynamics phenomena from micro-to nano-scale conjunctions", *Tribology International*, 2009, 42(11-12), pp. 1531-1541.
- [28] Hultqvist, T., Shirzadegan, M., Vrcek, A., Baubet, Y., Prakash, B., Marklund, P. and Larsson, R., "Elastohydrodynamic lubrication for the finite line contact under transient loading conditions", *Tribology International*, 2018, 127, pp. 489-499.
- [29] Qiu, L., Liu, S., Chen, X. and Wang, Z., "Lubrication and loading characteristics of cylindrical roller bearings with misalignment and roller modifications", *Tribology International*, 2022, 165:107291.
- [30] Teodorescu, M., Votsios, V., Rahnejat, H., "Fundamentals of impact dynamics of semi-infinite and layered solids", In *Tribology and Dynamics of Engine and Powertrain*, Woodhead Publishing, 2010, pp. 105-132e.
- [31] Gohar, R. and Rahnejat, H., "Fundamentals of Tribology", 3rd Edition, World Scientific Publishing, London, 2018.

- [32] Ioannides, E., "Tribology and rolling element bearings: the partnership continues", Donald Julius Groen Lecture, Institution of Mechanical Engineers, London, 2004.
- [33] Palmgren, A., "Ball and roller bearing engineering", Philadelphia: SKF Industries Inc., 1959.